Journal of Materials Chemistry C

PAPER

View Article Online
View Journal | View Issue

Cite this: J. Mater. Chem. C, 2018, 6, 12347

Enhanced open circuit voltage of small molecule acceptors containing angular-shaped indacenodithiophene units for P3HT-based organic solar cells†

Hongyan Huang,‡[ab] Bo Xiao,‡[cd] Chengting Huang,[a] Jing Zhang,[a] Shuli Liu,[a] Nina Fu,[a] Baomin Zhao,*[a] Tianshi Qin,[b] Erjun Zhou*[c] and Wei Huang*[ae]

Received 12th September 2018,
Accepted 22nd October 2018

DOI: 10.1039/c8tc04608e

rsc.li/materials-c

Angular indaceno[2,1-*b*:6,5-*b*′]dithiophene (**a-IDT**) as an analogue of linear-IDT (**l-IDT**), in which the central phenyl ring was linked to the β-position of the thiophene ring but fused on its α-position, was designed and exploited *via* intramolecular annulation. Two A–D–A type small molecule acceptors (SMAs) **l-IDTBTRh** and **a-IDTBTRh**, with **l-IDT** and **a-IDT** as the central cores, benzothiadiazole (BT) as the π-bridge acceptor segments and 3-ethylrhodanine as the end-capping groups, were synthesized and employed for P3HT-based fullerene free organic solar cells. The geometric shape of the **l-IDT** and **a-IDT** subunits plays a pivotal role in governing the optoelectronic properties, the charge mobility, the morphology and the photovoltaic performance of the resulting acceptors. Preliminarily, the device based on P3HT/l-IDTBTRh (1 : 08, w/w) displayed a circuit current density (J_{sc}) of 8.81 mA cm^{-2}, an open-circuit voltage (V_{oc}) of 0.86 V and a fill factor (FF) of 71.0%, delivering a decent PCE of 5.38%, which is associated with the lower bandgap, the better charge mobility and the morphology. Despite the inferior photovoltaic performance (2.53%), solar cells based on BHJ blends of **a-IDTBTRh** and P3HT offer a remarkably higher V_{oc} of 0.92 V as a result of the high-lying LUMO energy level (−3.59 eV), representing one of the highest values among the reported IDT-based A–D–A type SMAs for solar cells containing P3HT. The results suggested that introducing an **a-IDT** segment as the central core into A–D–A type SMAs can effectively increase the LUMO energy level of SMAs, offering an efficient strategy to design non-fullerene small molecule acceptors with high V_{oc} based-P3HT organic solar cells.

Introduction

Over the past few decades, the state-of-the-art bulk heterojunction (BHJ) organic solar cells (OSCs) containing polymer donors and fullerene derivatives as the acceptors have attracted widespread attention because of their low cost, lightweight and mechanical flexibility.[1–6] With the great endeavors devoted to the molecular engineering of the donor and acceptor materials, assisted by limited success in derivatizing the fullerene derivatives, the power conversion efficiency (PCE) of BHJ OSCs has exceeded 11%.[7–10] Fullerene derivatives have been prevailing acceptor materials in the development of BHJ OSCs owing to their isotropic electron transporting ability and high electron mobility. Nevertheless, fullerene derivatives suffer from intrinsic drawbacks, such as poor solubility and weak visible light absorption, high production cost and difficulty in energy level tuning, which makes it difficult to enhance the photovoltaic performance of BHJ OSCs.[11,12] Benefiting from the attraction of well-defined molecular structures, broad absorption and tunable energy levels, small molecule acceptors (SMAs) have become promising alternatives to fullerene derivatives.[13–18] PCEs over 17% have been realized for BHJ OSCs based on SMAs, surpassing their fullerene-based counterparts.[19]

[a] Key Laboratory for Organic Electronics and Information Displays, Jiangsu Key Laboratory for Biosensors, Institute of Advanced Materials (IAM), Jiangsu National Synergetic Innovation Center for Advanced Materials (SICAM), Nanjing University of Posts and Telecommunications, 9 Wenyuan Road, Nanjing 210023, China. E-mail: iambmzhao@njupt.edu.cn, wei-huang@njtech.edu.cn
[b] Key Laboratory of Flexible Electronics (KLOFE), Institute of Advanced Materials (IAM), Jiangsu National Synergetic Innovation Center for Advanced Materials (SICAM), Nanjing Tech University (Nanjing Tech), 30 South Puzhu Road, Nanjing 211816, China
[c] CAS Key Laboratory of Nanosystem and Hierarchical Fabrication, CAS Center for Excellence in Nanoscience, National Center for Nanoscience and Technology, Beijing 100190, China. E-mail: zhouej@nanoctr.cn
[d] University of Chinese Academy of Sciences, Beijing 100049, P. R. China
[e] Shaanxi Institute of Flexible Electronics (SIFE), Northwestern Polytechnical University (NPU), Xi'an 710072, China

† Electronic supplementary information (ESI) available: TGA spectra, NMR spectra, and device optimization. See DOI: 10.1039/c8tc04608e

‡ H. Y. Huang and B. Xiao contributed equally to this work.

To date, SMAs with acceptor–donor–acceptor (A–D–A) architectures, where the donor unit (D) as the central core can be combined with a wide variety of electron-withdrawing groups (A), have been the preferred acceptors for high-performance BHJ OSCs.[13–15] The pentacyclic indaceno[2,1-*b*:6,5-*b*′]dithiophene (IDT) unit, as a thiophene-fused heteroarene, with two thiophene rings fused with the central phenyl ring into linear pentacyclic aromatics, represents one of the most prospective motifs for constructing SMAs due to its rigidity and planarity.[17,20–25] Additionally, the peripheral substituents on the IDT backbones can not only ensure high solution processability of IDT-based acceptors but also suppress their aggregation in solid states. Sharing these chemical structural features, a series of A–D–A type SMAs that utilize IDT units as the core and different electron-withdrawing units as end-capping groups were developed recently. Considerable efforts have been devoted to modifying the molecular structures through side chain engineering,[26,27] backbone conjugation regulation,[28–32] heteroatom substitution,[33] π-bridge acceptor modulation,[34–40] and choosing end-capping acceptor segments.[38,41,42] However, less attention has been paid to the geometric shape of the IDT unit as well as its A–D–A type SMAs. Note that naphthodithiophene (NDT), another thiophene-fused heteroarene, can be categorized into linear-shaped NDT (**l-NDT**) and angular-shaped NDT (**a-NDT**) depending on the geometry of the fused thiophenes and a wide variety of NDT-based organic semiconductor materials have been developed for organic field-effect transistor (OFET) and OSC applications.[43–48] Besides, A–D–A type SMAs based on **a-NDT** have been reported and successfully applied to ternary blend OSCs.[49] Similarly, the IDT unit should also possess angular and linear configurations of angular-IDT (**a-IDT**) and linear-IDT (**l-IDT**), where either the α- or β-positions of the thiophene units are attached to the central phenyl moiety.

On the other hand, many D–A type copolymers have been selected as donor materials for high-performance non-fullerene BHJ OSCs.[18–20,50] Compared to these copolymers, the simplest homopolymer of poly(3-hexylthiophene) (P3HT) can be easily synthesized at low cost, demonstrating that P3HT has become the most representative and promising donor polymer for BHJ OSC applications.[51–53] However, P3HT possesses a high-lying HOMO energy level (around −5.00 eV), resulting in a low open-circuit voltage (V_{oc}) (around 0.6 V) for the P3HT/PCBM system. Therefore, the exploitation of novel A–D–A type SMAs having high-lying LUMO energy level for improving V_{oc} in P3HT-based BHJ OSCs is vital. For the first time, Zhan's group reported A–D–A type SMAs containing IDT as the central donor core and successfully applied them to P3HT-based BHJ OSCs.[24,25] Very recently, Zhou's group has made significant achievements for improving V_{oc} in P3HT-based BHJ OSCs,[34–36,40] more notably, they have developed the small molecule acceptor BTA2 containing IDT and realized a double V_{oc} of 1.22 V compared to that of the $PC_{61}BM$-based control device (about 0.6 V) when blending with the donor material of P3HT.[35]

On account of the aforementioned considerations, it is of great interest to design new A–D–A SMAs containing IDT units for improving V_{oc} in P3HT-based BHJ OSCs. We have focused on the design and synthesis of the materials for OFETs and BHJ OSCs.[54–60] And we have recently exploited three A–D–A SMAs including *N*-annulated perylene diimide, and the non-fullerene BHJ OSCs could achieve a high V_{oc} of 1.14 V.[60] Inspired by our previous work, herein, **a-IDT** as an analogue of **l-IDT**, in which the central phenyl ring was linked to the β-position of the thiophene ring but fused on its α-position, was designed and developed *via* intramolecular annulation for the first time (Fig. 1). Two A–D–A type SMAs **l-IDTBTRh** and **a-IDTBTRh** (Fig. 1), with **l-IDT** and **a-IDT** as the central cores, benzothiadiazole (BT) as the π-bridge acceptor moiety and 3-ethylrhodanine as the end-capping group, were synthesized and employed for P3HT-based non-fullerene organic solar cells. The effects of the geometric shapes of the **l-IDT** and **a-IDT** subunits on the thermal, optical, electrochemical and film-forming properties, the charge mobility and the photovoltaic performance of the resulting acceptors were investigated. A preliminary photovoltaic study of P3HT/SMA blend films was conducted for exploring their potential applications in non-fullerene BHJ OSCs.

Results and discussion

Synthesis and thermal properties

The synthetic routes and details of the small molecule acceptors are shown in Scheme 1 and in the ESI.† Compounds **2** and **3**

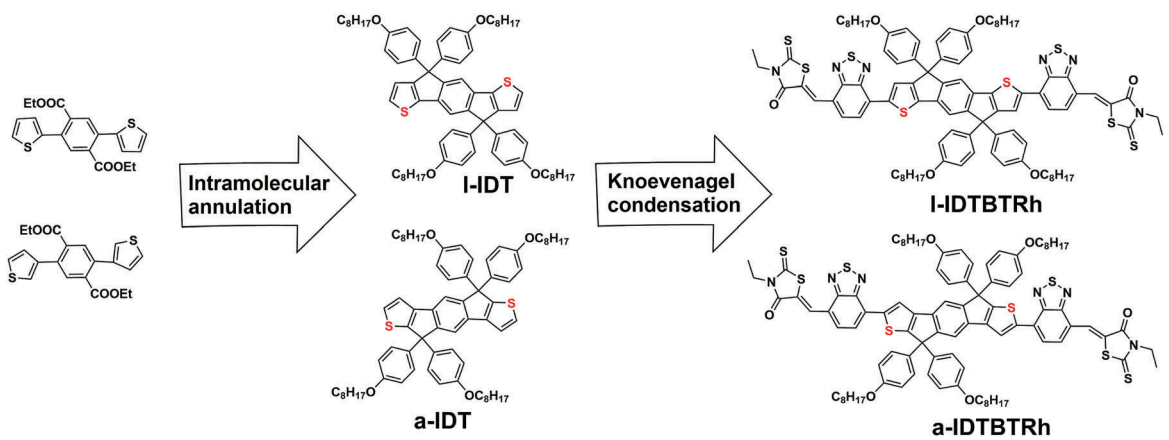

Fig. 1 Chemical structures of **l-IDT**, **a-IDT** and **l-IDTBTRh**, **a-IDTBTRh**.

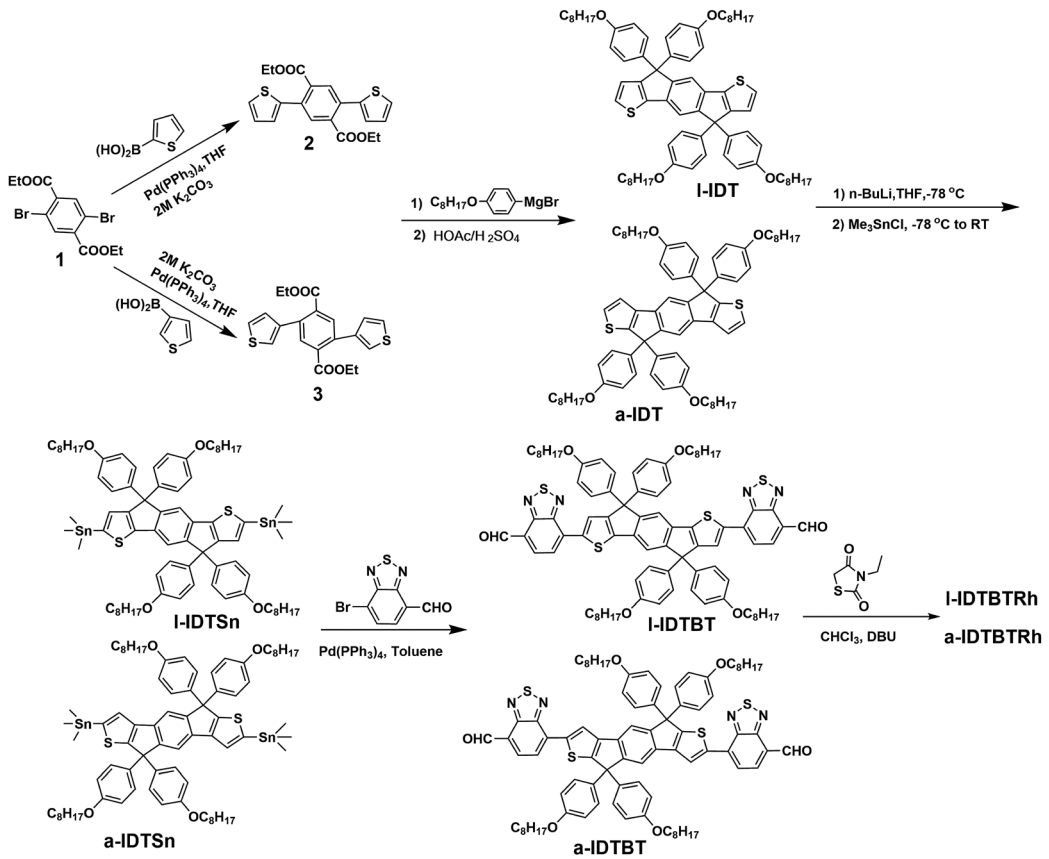

Scheme 1 Synthetic routes to **l-IDTBTRh** and **a-IDTBTRh**.

were synthesized using the Suzuki reaction between diethyl 2,5-dibromoterephthalate (**1**) and 2-thiophenylboric acid, 3-thiophenylboric acid with a yield of 73% and 64%, respectively. In order to improve the solubility of the conjugated polymers and suppress the aggregation, alkyl side chains that incorporated *p*-(octyloxy)phenyl derivatives were introduced. **l-IDT** and **a-IDT** were synthesized by following the reported procedure through the addition of *p*-(octyloxy)phenyl Grignard reagent into a solution of compounds **2** and **3** containing the ester to give the corresponding alcohol and then cyclized subsequently through the acid-mediated reaction.[61] By treating the compounds **l-IDT** and **a-IDT** with *n*-butyllithium (*n*-BuLi), followed by adding trimethyltin chloride, l-IDTSn and a-IDTSn were obtained *via* rotary evaporation and directly used for the next step without any treatment. **l-IDTBT** and **a-IDTBT** as the important intermediates were synthesized using the Stille coupling reaction with $Pd(PPh_3)_4$ as the catalyst and toluene as the solvent.[62] Finally, the target small acceptor molecules **l-IDTBTRh** and **a-IDTBTRh** were obtained by the Knoevenagel condensation of compounds **l-IDTBT** and **a-IDTBT** with 3-ethylrhodanine, respectively. The chemical structures of the intermediates and the target small acceptor molecules were confirmed *via* ^{1}H NMR and ^{13}C NMR spectroscopy and MALDI-TOF MS (Fig. S3–S10, ESI†). Both the small acceptor molecules exhibited excellent solubility at room temperature in common organic solvents, such as tetrahydrofuran (THF), chloroform (CF) and chlorobenzene (CB). Additionally, the thermal properties of these small acceptor molecules were evaluated by thermogravimetric analysis (TGA). As shown in Fig. S1 (ESI†) and Table 1, the 5% weight loss temperature is 376 and 389 °C for **l-IDTBTRh** and **a-IDTBTRh**, respectively, indicating that the two small acceptor molecules exhibited excellent stability and meet the requirements of fabricating organic solar cell devices.

Table 1 Optical and electrochemical properties of **l-IDTBTRh** and **a-IDTBTRh**

		Solution[b]		Film[c]				
Compound	T_d[a] (°C)	λ_{max} (nm)	ε (M^{-1} cm^{-1})	λ_{max} (nm)	λ_{edge} (nm)	E_g^{opt}[d] (eV)	E_{onset}^{ox} (V)/HOMO (eV)	E_{onset}^{red} (V)/LUMO (eV)
l-IDTBTRh	376	618	9×10^4	667	751	1.65	1.02/−5.42	−0.72/−3.68
a-IDTBTRh	389	548	5.3×10^4	570	653	1.89	1.23/−5.63	−0.81/−3.59

[a] The 5% weight-loss temperatures under a nitrogen atmosphere. [b] Measured in dilute dichloromethane solution. [c] Cast from dichloromethane solution. [d] Bandgap estimated from the onset wavelength (λ_{edge}) of the optical absorption: $E_g^{opt} = 1240/\lambda_{edge}$.

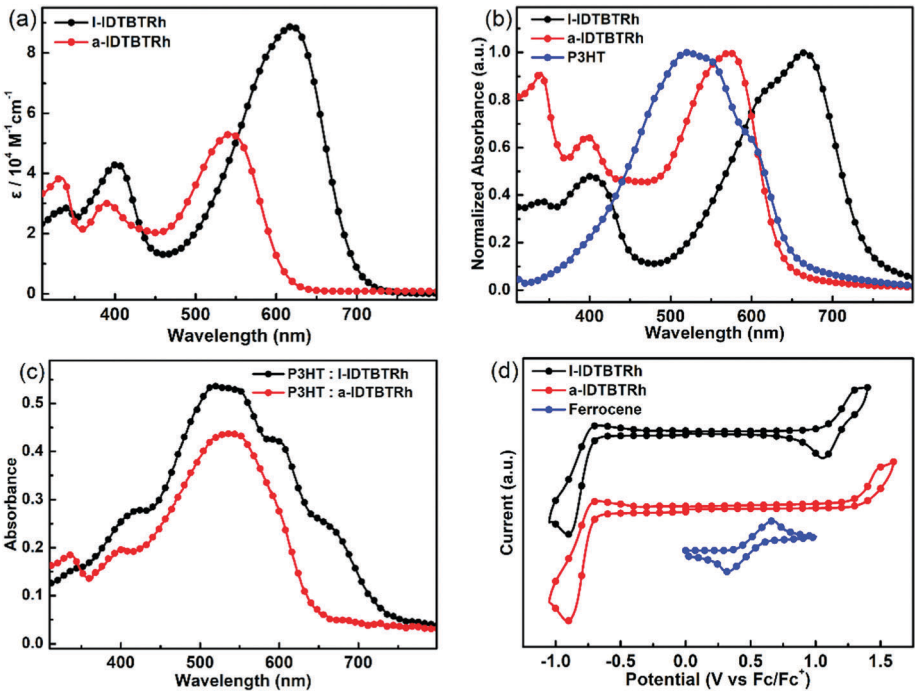

Fig. 2 (a) Absorption spectra of **l-IDTBTRh** and **a-IDTBTRh** in solution, (b) absorption spectra of **l-IDTBTRh**, **a-IDTBTRh** and P3HT in thin films, (c) absorption spectra of the blend films P3HT : l-IDTBTRh (1 : 0.8, w/w) and P3HT : a-IDTBTRh (0.8 : 1, w/w), and (d) cyclic voltammograms of **l-IDTBTRh** and **a-IDTBTRh** recorded from solution at a scan rate of 50 mV s^{-1}.

Optical properties

Fig. 2 shows the absorption spectra of the small molecule acceptors **l-IDTBTRh** and **a-IDTBTRh**, respectively, where the solution spectrum was measured in dilute dichlorobenzene and the thin films were prepared by spin-coating the dichlorobenzene solution on the quartz glass substrate. The related optical data including the maximum absorption peak (λ_{max}), the absorption edge (λ_{edge}), the molar absorption coefficient (ε) and the optical band gap (E_g^{opt}) are summarized in Table 1. As shown in Fig. 2a and b, for the two small molecule acceptors, the absorption spectra were mainly dependent on the geometric shapes of the **l-IDT** and **a-IDT** subunits. In dilute solution, the molar extinction coefficients of **l-IDTBTRh** and **a-IDTBTRh** were 9×10^4 M^{-1} cm^{-1} and 5.3×10^4 M^{-1} cm^{-1}, and the maximum absorption peaks in the long wavelength regions which were located at 618 nm for **l-IDTBTRh** and 548 nm for **a-IDTBTRh**, respectively, correspondingly red-shifted to 667 nm and 570 nm for their spectra in thin films, which may be attributed to the stronger intermolecular interactions formed in the thin films. Moreover, the spectrum of **l-IDTBTRh** showed a significantly red-shifted absorption compared to that of **a-IDTBTRh**, suggesting that the **l-IDT** moiety may induce more effective conjugation than the **a-IDT** segment and thus stronger π–π stacking existed in **l-IDTBTRh**. Optical bandgaps (E_g^{opt}) deduced from the absorption edges of the thin film spectra were determined to be 1.65 eV for **l-IDTBTRh** and 1.89 eV for **a-IDTBTRh**. The absorption spectra of the blend films are shown in Fig. 2c, and the spectral features of the two small molecule acceptors exhibited some complementary with the absorption of P3HT as the donor material. In particular, the blend films of l-IDTBTRh/P3HT displayed stronger and broader absorption than those of a-IDTBTRh/P3HT, benefitting from absorbing more photons and generating high photocurrent.

Electrochemical properties

It is well known that the matched energy levels between the donor and acceptor materials are very important for high-performance organic solar cells. Cyclic voltammetry (CV) with Ag/AgCl as a reference electrode and the Fc/Fc^+ couple as an internal reference was executed to determine the energy levels of the two small molecule acceptors. The CV curves are shown in Fig. 2d and the related electrochemical data are summarized in Table 1. The HOMO and LUMO levels were calculated from the onset potentials (E_{onset}^{ox}) and reduction potentials (E_{onset}^{red}), respectively. The HOMO/LUMO energy levels were −5.42/−3.68 eV for **IDTBTRh** and −5.63/−3.59 eV for **a-IDTBTRh**, respectively, corresponding with those of wide-bandgap polymer donors such as P3HT to guarantee efficient exciton dissociation. Their LUMO levels of the two small molecule acceptors are higher than those of $PC_{61}BM$ (~3.9 eV), and thus a higher V_{oc}, especially **a-IDTBTRh** should be expected in P3HT-based BHJ OSCs. The results demonstrate that the geometric shape of the **l-IDT** and **a-IDT** subunits also exerts notable effects on the energy level for the resulting acceptors and **a-IDT** may be a good choice to design A–D–A type SMAs with an upshifted LUMO energy level for increasing V_{oc} in P3HT-based BHJ OSCs. The electrochemical energy gaps (E_g^{ec}) were estimated to be 1.74 eV for **l-IDTBTRh** and 2.04 eV for **a-IDTBTRh**, which are larger than their corresponding E_g^{opt} in the thin films.

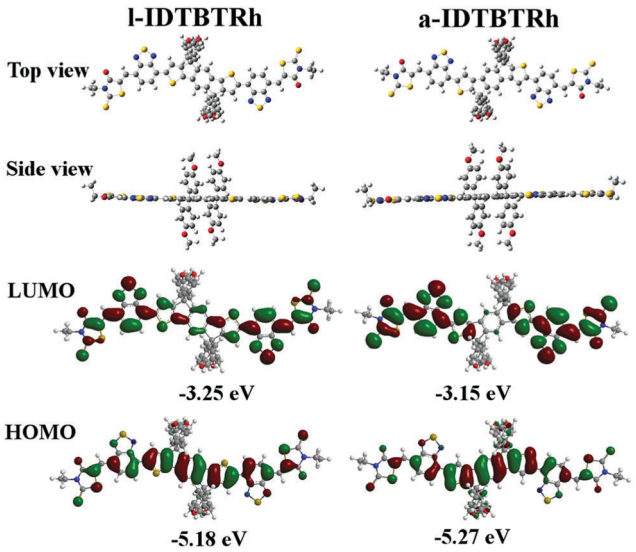

Fig. 3 Simulated molecular geometries obtained by DFT calculations for simplified molecules of **l-IDTBTRh** and **a-IDTBTRh**.

Theoretical calculations

Density functional theory (DFT) calculations were carried out using the Gaussian 09 program at the B3LYP/6-31G level of theory to investigate the molecular geometry and molecular frontier orbitals for **l-IDTBTRh** and **a-IDTBTRh**. All alkyl side chains were replaced by methyl groups to save the time required for calculations. As shown in Fig. 3, the two small molecules **l-IDTBTRh** and **a-IDTBTRh** adopt nearly flat backbone configurations, thus facilitating the charge transport. The octyloxyphenyl groups on the **l-IDT** moiety exhibited a dihedral angle about 117° to the backbone plane for **l-IDTBTRh**, similarly to **a-IDTBTRh** (about 119°), which is conducive to the formation of the interpenetrating networks and the phase separation when blending with P3HT as the donor material. Clearly, a similar HOMO energy distribution was observed for **l-IDTBTRh** and **a-IDTBTRh**, and mainly located along the whole molecule skeletons. However, the LUMO energy distributions of the two small molecules were obviously different. For **a-IDTBTRh**, the electron density of the LUMO orbital was mainly positioned on the BT unit, the linked double bond and the terminal acceptor, whereas that of **l-IDTBTRh** was localized along the whole molecule skeleton, indicating that the geometric shape of the **l-IDT** and **a-IDT** subunits has an impact on the LUMO energy distribution of the resulting small molecule acceptors. The calculated HOMO/LUMO energy levels were −5.18/−3.25 eV for **l-IDTBTRh** and −5.27/−3.15 eV for **a-IDTBTRh**. The limited electron density delocalization of the LUMO energy could be responsible for the slightly higher LUMO energies of **a-IDTBTRh** than **l-IDTBTRh**. The trend in the variation of the energy levels agreed well with those obtained from the CV measurements.

Photovoltaic properties and mobility

To evaluate the photovoltaic properties of **l-IDTBTRh** and **a-IDTBTRh** as the acceptor materials, the BHJ OSC devices with a conventional configuration of ITO/PEDOT:PSS/P3HT : l-IDTBTRh or **a-IDTBTRh**/Ca/Al using P3HT as the donor material were fabricated (Fig. S2, ESI†). The *J*–*V* curves and the relevant parameters such as short circuit current density (J_{sc}), V_{oc} and fill factor (FF) are shown in Fig. 4a and Table 2. More detailed device parameters are provided in the ESI† (Tables S1–S4). The optimal

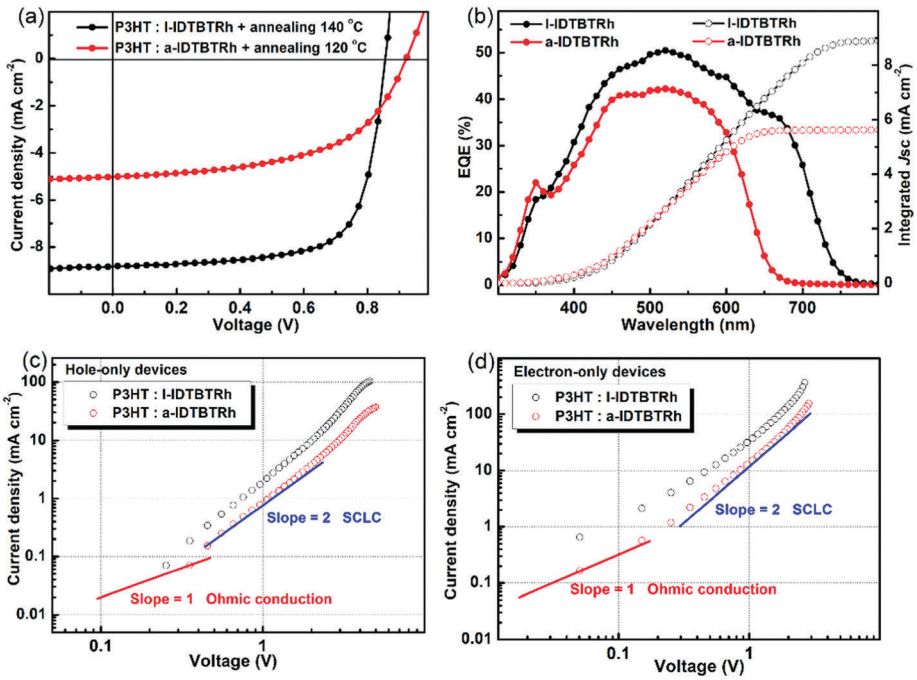

Fig. 4 (a) *J*–*V* curves based on P3HT : l-IDTBTRh (1 : 0.8, w/w) and P3HT : a-IDTBTRh (0.8 : 1, w/w) as the active layers upon thermal annealing treatment. (b) The EQE profiles and the corresponding integrated J_{sc} of the organic solar cells in structures of ITO/PEDOT:PSS/P3HT : l-IDTBTRh (1 : 0.8, w/w) or P3HT : a-IDTBTRh (0.8 : 1, w/w)/Ca/Al. (c) The *J*–*V* curves of the hole-only devices. (d) The *J*–*V* curves of the electron-only devices.

Table 2 Photovoltaic performances of the organic solar cells based on P3HT/l-IDTBTRh or **a-IDTBTRh** under the illumination of AM 1.5 G, 100 mW cm^{-2}

Blend	D/A (w/w)	J_{sc} (mA cm^{-2})	V_{oc} (V)	FF (%)	PCE (%)	μ_h (cm^2 V^{-1} s^{-1})	μ_e (cm^2 V^{-1} s^{-1})
P3HT:l-IDTBTRh[a]	1 : 0.8	8.81 (8.84)[c]	0.86	71.0	5.38	2.32×10^{-6}	1.15×10^{-5}
P3HT:a-IDTBTRh[b]	0.8 : 1	5.00 (4.87)[c]	0.92	55.0	2.53	1.46×10^{-6}	8.84×10^{-6}

[a] Thermal annealing at 140 °C for 10 min. [b] Thermal annealing at 120 °C for 10 min. [c] Integrated from EQE data.

conditions for the device fabrication were carefully screened by choosing the D/A ratio, the spin-coating speed, the solvent, the thermal annealing temperature and solvent additives. The optimal D/A weight ratios were found to be 1 : 0.8 for P3HT/l-IDTBTRh and 0.8 : 1 for P3HT/a-IDTBTRh, and the optimal thermal annealing temperatures were 140 °C and 120 °C for P3HT/l-IDTBTRh and P3HT/a-IDTBTRh, respectively. As shown in Fig. 4a and Table 2, the P3HT/l-IDTBTRh based device displayed a decent PCE of 5.38% with a J_{sc} of 8.81 mA cm^{-2}, a V_{oc} of 0.86 V, and a remarkable FF of 71.0%, which may stem from the strong and broad light-harvesting range as well as the balanced charge carrier transport. With respect to P3HT/a-IDTBTRh,a J_{sc} of 5.00 mA cm^{-2}, a V_{oc} of 0.92 V, a FF of 55.0% and an inferior PCE of 2.53% were delivered. The angular- or linear-shape of the IDT subunits results in different photovoltaic performances of the small molecule acceptors. It should be noted that these devices yielded a higher V_{oc} (> 0.82 V) than that of $PC_{61}BM$-based control devices (~0.6 V), especially for P3HT/a-IDTBTRh, a V_{oc} of 0.92 V was obtained, which is one of the highest values among the reported IDT based A–D–A type SMAs. Generally, solvent additives, such as 1,8-diiodooctane (DIO), diphenyl ether (DPE), and 1-chloronaphthalene (CN), were employed to optimize the morphology and thus improve the photovoltaic performance.[63] Disappointingly, as shown in Table S4 (ESI†), these solvent additives could not improve the photovoltaic performance of P3HT/l-IDTBTRh and P3HT/a-IDTBTRh.

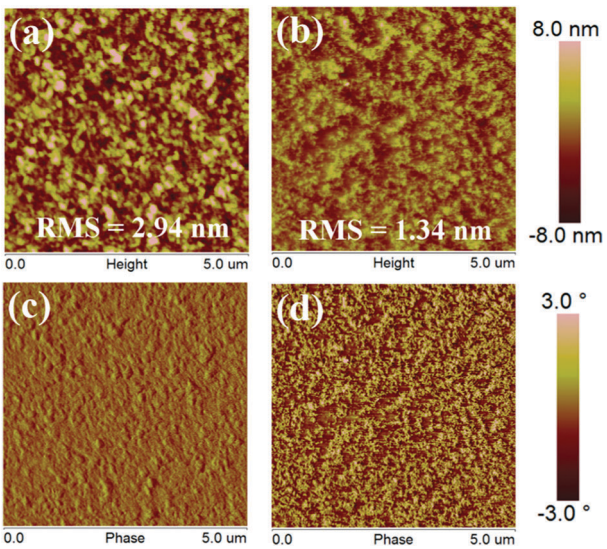

Fig. 5 AFM height (a and b) and phase (c and d) images of blend films upon thermal treatment: (a and c) P3HT : l-IDTBTRh (1 : 0.8, w/w); (b and d) P3HT : a-IDTBTRh (0.8 : 1, w/w).

The surface morphology of the blend films was explored by atomic force microscopy (AFM). As shown in Fig. 5, the root-mean-square (RMS) roughness values are 2.94 nm for P3HT/l-IDTBTRh and 1.34 nm for P3HT/a-IDTBTRh, respectively. As usual, too large or small phase separation in the blend film is not conducive to the charge separation and transport, resulting in the reduction of J_{sc} and FF. Therefore, the lower RMS value of the blend film P3HT/a-IDTBTRh may be responsible for the lower J_{sc}, FF and photovoltaic performance.

For insights into the charge transport properties of the two small molecule acceptors, the charge mobilities of the optimized P3HT/l-IDTBTRh and P3HT/a-IDTBTRh blend films were measured by the space charge limited current (SCLC) method. The hole mobility (μ_h) and electron mobility (μ_e) were acquired from the device configuration of ITO/PEDOT:PSS/active layer/Au and ITO/titanium(diisopropoxide)bis(2, 4-pentanedionate), 75% in isopropanol liquid (TIPD)/active layer/Al, respectively. As shown in Fig. 4c and d, the as-cast blend films of P3HT and **a-IDTBTRh** exhibited a μ_h of 1.46×10^{-6} cm^2 V^{-1} s^{-1} and a μ_e of 8.84×10^{-6} cm^{-2} V^{-1} s^{-1}, whereas the blend films of P3HT/l-IDTBTRh showed a slightly higher μ_h of 2.32×10^{-6} cm^2 V^{-1} s^{-1} and μ_e of 1.15×10^{-5} cm^2 V^{-1} s^{-1}. Additionally, a more balanced μ_e/μ_h (4.96) of the P3HT/l-IDTBTRh blend film is achieved than that of the P3HT/a-IDTBTRh blend film (6.05). The results indicate that P3HT/l-IDTBTRh possesses a higher and more balanced charge mobility, which could partly explain the enhanced J_{sc}, FF and photovoltaic performance in OSCs compared to P3HT/a-IDTBTRh.

The trend of the mobilities of the two blend films is consistent well with their PCE values.

The external quantum efficiency (EQE) plots of **l-IDTBTRh** and **a-IDTBTRh** based on the optimized BHJ OSCs are shown in Fig. 4b. The EQE curve of the OSCs based on a-IDTBTRh/P3HT (0.8 : 1, w/w) covered a broad wavelength range from 300 to 650 nm with the maximum EQE value of 42% at *ca.* 520 nm, while the EQE curve of the organic solar cell based on l-IDTBTRh/P3HT (1 : 0.8, w/w) exhibited a higher EQE value of 51% at 522 nm and a broader wavelength range. The higher EQE values of the organic solar cell based on **l-IDTBTRh** agree with the higher J_{sc} of the device mentioned above. The J_{sc} values calculated from integration of the EQE spectra with the AM 1.5 G reference spectrum are 8.84 mA cm^{-2} for **l-IDTBTRh** and 4.87 mA cm^{-2} for **a-IDTBTRh**, which is in accord with those obtained from *J–V* measurements.

Conclusions

In summary, we have successfully developed angular-shaped **a-IDT** as the analogue of **l-IDT** *via* intramolecular annulation,

in which the central phenyl ring was linked to the β-position of the thiophene ring but fused on its α-position. Two A–D–A type SMAs **l-IDTBTRh** and **a-IDTBTRh** with **l-IDT** and **a-IDT** as the central cores were also synthesized and employed for P3HT-based organic solar cells. The geometric shape of the **l-IDT** and **a-IDT** subunits plays a pivotal role in governing the optoelectronic properties, the charge mobility, the morphology and the photovoltaic performance of the resulting acceptors. Both small molecule acceptors possessed excellent thermal stability and solubility in common organic solvents and adopted nearly flat backbone configurations. Compared to **a-IDTBTRh**, **l-IDTBTRh** exhibited a lower bandgap and better charge mobility and morphology. By blending with P3HT, BHJ OSCs delivered a decent PCE of 5.38% with a higher J_{sc} of 8.81 mA cm^{-2} and a FF of 71.0% for **l-IDTBTRh**. Although displaying an inferior photovoltaic performance (2.53%), solar cells based on BHJ blends of **a-IDTBTRh** and P3HT offer a remarkably high V_{oc} of 0.92 V as a result of the upshifted LUMO energy level (−3.59 eV), which is one of the highest values among the reported IDT based A–D–A type SMAs. Our work demonstrates that **a-IDT** is an effective building block to construct promising A–D–A SMAs with high-lying LUMO energy levels, providing a strategy to increase V_{oc} in P3HT-based organic solar cells.

Conflicts of interest

There are no conflicts to declare.

Acknowledgements

This research was financially supported by the National Key Research and Development Program of China (2017YFB0404501), the National Basic Research Program of China-Fundamental Studies of Perovskite Solar Cells (2015CB932200), the Priority Academic Program Development of Jiangsu Higher Education Institutions (PAPD) and the Program for Changjiang Scholars and Innovative Research Team in University (IRT-15R37), and the NJUPT Culturing Project (NY214080, NY214087 and NY218056).

References

1 G. Li, R. Zhu and Y. Yang, *Nat. Photonics*, 2012, **6**, 153–161.
2 A. J. Heeger, *Adv. Mater.*, 2014, **26**, 10–28.
3 D. Landerer, A. Mertens, D. Freis, R. Droll, T. Leonhard, A. D. Schulz, D. Bahro and A. Colsmann, *njp Flexible Electron.*, 2017, **1**, 11.
4 L. Lu, T. Zheng, Q. Wu, A. M. Schneider, D. L. Zhao and L. P. Yu, *Chem. Rev.*, 2015, **115**, 12666–12731.
5 P. Cheng, G. Li, X. W. Zhan and Y. Yang, *Nat. Photonics*, 2018, **12**, 131–142.
6 C. Liu, K. Wang, X. Gong and J. H. Alan, *Chem. Soc. Rev.*, 2016, **45**, 4825–4846.
7 H. Q. Zhou, Y. Zhang, C. K. Mai, D. Samuel, S. D. Collins, G. C. Bazan, T.-Q. Nguyen and A. J. Heeger, *Adv. Mater.*, 2015, **27**, 1767–1773.
8 J. Zhao, Y. Li, G. Yang, K. Jiang, H. Lin, H. Ade, W. Ma and H. Yan, *Nat. Energy*, 2016, **1**, 15027.
9 J. Wan, X. Xu, G. Zhang, Y. Li, K. Feng and Q. Peng, *Energy Environ. Sci.*, 2017, **10**, 1739–1745.
10 D. Deng, Y. Zhang, J. Zhang, Z. Wang, L. Zhu, J. Fang, B. Xia, Z. Wang, K. Lu, W. Ma and Z. Wei, *Nat. Commun.*, 2016, **7**, 13740.
11 W. Chen and Q. Zhang, *J. Mater. Chem. C*, 2017, **5**, 1275–1302.
12 S. X. Li, W. Q. Liu, C. Z. Li, M. M. Shi and H. Z. Chen, *Small*, 2017, **13**, 1701120.
13 J. Hou, O. Inganäs, R. H. Friend and F. Gao, *Nat. Mater.*, 2018, **17**, 119–128.
14 Y. Yang, Z. G. Zhang, H. Bin, S. Chen, L. Gao, L. Xue, C. Yang and Y. Li, *J. Am. Chem. Soc.*, 2016, **138**, 15011–15018.
15 P. Cheng, G. Li, X. Zhan and Y. Yang, *Nat. Photonics*, 2018, **12**, 131–142.
16 S. Dai, F. Zhao, Q. Zhang, T.-K. Lau, T. Li, K. Liu, Q. Ling, C. Wang, X. Lu, W. You and X. Zhan, *J. Am. Chem. Soc.*, 2017, **139**, 1336–1343.
17 Y. Liu, Z. Zhang, S. Feng, M. Li, L. Wu, R. Hou, X. Xu, X. Chen and Z. Bo, *J. Am. Chem. Soc.*, 2017, **139**, 3356–3359.
18 Y. Lin, F. Zhao, Q. He, L. Huo, Y. Wu, T. C. Parker, W. Ma, Y. Sun, C. Wang, D. Zhu, A. J. Heeger, S. R. Marder and X. Zhan, *J. Am. Chem. Soc.*, 2016, **138**, 4955–4961.
19 M. Li, Y. Zhang, X. Wan, C. Li, X. Zhang, Y. Wang, X. Ke, Z. Xiao, L. Ding, R. Xia, H. Yip, Y. Cao and Y. Chen, *Science*, 2018, eaat2612.
20 Y. Lin, Q. He, F. Zhao, L. Huo, J. Mai, X. Lu, C. J. Su, T. Li, J. Wang, J. Zhu, Y. Sun, C. Wang and X. Zhan, *J. Am. Chem. Soc.*, 2016, **138**, 2973–2976.
21 S. Holliday, R. S. Ashraf, A. Wadsworth, D. Baran, S. A. Yousaf, C. B. Nielsen, C. H. Tan, S. D. Dimitrov, Z. Shang, N. Gasparini, M. Alamoudi, F. Laquai, C. J. Brabec, A. Salleo, J. R. Durrant and I. McCulloch, *Nat. Commun.*, 2016, **7**, 1–11.
22 Y. Wu, H. Bai, Z. Wang, P. Cheng, S. Zhu, Y. Wang, W. Ma and X. Zhan, *Energy Environ. Sci.*, 2015, **8**, 3215–3221.
23 Y. Lin, Z. G. Zhang, H. Bai, J. Wang, Y. Yao, Y. Li, D. Zhu and X. Zhan, *Energy Environ. Sci.*, 2015, **8**, 610–616.
24 Y. Lin, J. Wang, S. Dai, Y. Li, D. Zhu and X. Zhan, *Adv. Energy Mater.*, 2014, **4**, 2–6.
25 H. Bai, P. Cheng, Y. Wang, L. Ma, Y. Li, D. Zhu and X. Zhan, *J. Mater. Chem. A*, 2014, **2**, 778–784.
26 B. Jia, Y. Wu, F. Zhao, C. Yan, S. Zhu, P. Cheng, J. Mai, T. K. Lau, X. Lu, C. J. Su, C. Wang and X. Zhan, *Sci. China: Chem.*, 2017, **60**, 257–263.
27 Y. Cai, X. Zhang, X. Xue, D. Wei, L. Huo and Y. Sun, *J. Mater. Chem. C*, 2017, **5**, 7777–7783.
28 W. Wang, C. Yan, T. K. Lau, J. Wang, K. Liu, Y. Fan, X. Lu and X. Zhan, *Adv. Mater.*, 2017, **29**, 1–7.
29 Y. Lin, J. Wang, Z.-G. Zhang, H. Bai, Y. Li, D. Zhu and X. Zhan, *Adv. Mater.*, 2015, **27**, 1170–1174.
30 B. Jia, S. Dai, Z. Ke, C. Yan, W. Ma and X. Zhan, *Chem. Mater.*, 2018, **30**, 239–245.
31 Y. Li, X. Liu, F.-P. Wu, Y. Zhou, Z.-Q. Jiang, B. Song, Y. Xia, Z.-G. Zhang, F. Gao, O. Inganäs, Y. Li and L.-S. Liao, *J. Mater. Chem. A*, 2016, **4**, 5890–5897.

32 Y. Lin, F. Zhao, Q. He, L. Huo, Y. Wu, T. C. Parker, W. Ma, Y. Sun, C. Wang, D. Zhu, A. J. Heeger, S. R. Marder and X. Zhan, *J. Am. Chem. Soc.*, 2016, **138**, 4955–4961.
33 Y. Li, L. Zhong, F. P. Wu, Y. Yuan, H. J. Bin, Z. Q. Jiang, Z. Zhang, Z. G. Zhang, Y. Li and L. S. Liao, *Energy Environ. Sci.*, 2016, **9**, 3429–3435.
34 B. Xiao, A. Tang, J. Zhang, A. Mahmood, Z. Wei and E. Zhou, *Adv. Energy Mater.*, 2017, **7**, 1–7.
35 B. Xiao, A. Tang, J. Yang, Z. Wei and E. Zhou, *ACS Macro Lett.*, 2017, **6**, 410–414.
36 B. Xiao, A. Tang, J. Yang, A. Mahmood, X. Sun and E. Zhou, *ACS Appl. Mater. Interfaces*, 2018, **10**, 10254–10261.
37 H. Yao, Y. Chen, Y. Qin, R. Yu, Y. Cui, B. Yang, S. Li, K. Zhang and J. Hou, *Adv. Mater.*, 2016, **28**, 8283–8287.
38 A. Mahmood, J. Hu, A. Tang, F. Chen, X. Wang and E. Zhou, *Dyes Pigm.*, 2018, **149**, 470–474.
39 Q. Y. Li, J. Xiao, L. M. Tang, H. C. Wang, Z. Chen, Z. Yang, H. L. Yip and Y. X. Xu, *Org. Electron.*, 2017, **44**, 217–224.
40 B. Xiao, A. Tang, L. Cheng, J. Zhang, Z. Wei, Q. Zeng and E. Zhou, *Sol. RRL*, 2017, **1**, 1700166.
41 Y. Cui, H. Yao, B. Gao, Y. Qin, S. Zhang, B. Yang, C. He, B. Xu and J. Hou, *J. Am. Chem. Soc.*, 2017, **139**, 7302–7309.
42 R. Li, G. Liu, M. Xiao, X. Yang, X. Liu, Z. Wang, L. Ying, F. Huang and Y. Cao, *J. Mater. Chem. A*, 2017, **5**, 23926–23936.
43 S. Shinamura, I. Osaka, E. Miyazaki, A. Nakao, M. Yamagishi, J. Takeya and K. Takimiya, *J. Am. Chem. Soc.*, 2011, **133**, 5024–5035.
44 S. Cheng, D. Chiou, Y. Lai, R. Yu, C. Lee and Y. Cheng, *Org. Lett.*, 2013, **15**, 5338–5341.
45 S. Shi, X. Xie, P. Jiang, S. Chen, L. Wang, M. Wang, H. Wang, X. Li, G. Yu and Y. Li, *Macromolecules*, 2013, **46**, 3358–3366.
46 S. Shi, P. Jiang, S. Yu, L. Wang, X. Wang, M. Wang, H. Wang, Y. Li and X. Li, *J. Mater. Chem. A*, 2013, **1**, 1540–1543.
47 S. W. Cheng, C. E. Tsai, W. W. Liang, Y. L. Chen, F. Y. Cao, C. S. Hsu and Y. J. Cheng, *Macromolecules*, 2015, **48**, 2030–2038.
48 D. Y. Chiou, F. Y. Cao, J. Y. Hsu, C. E. Tsai, Y. Y. Lai, U. S. Jeng, J. Zhang, H. Yan, C. J. Su and Y. J. Cheng, *Polym. Chem.*, 2017, **8**, 2334–2345.
49 F. Y. Cao, W. C. Huang, S. L. Chang and Y. J. Cheng, *Chem. Mater.*, 2018, **30**, 4968–4977.
50 D. Meng, D. Sun, C. M. Zhong, T. Liu, B. B. Fan, L. J. Huo, Y. Li, W. Jiang, H. Choi, T. Kim, J. Y. Kim, Y. M. Sun, Z. H. Wang and A. J. Heeger, *J. Am. Chem. Soc.*, 2016, **138**, 375–380.
51 M. T. Dang, L. Hirsch and G. Wantz, *Adv. Mater.*, 2011, **23**, 3597–3602.
52 R. Po, A. Bernardi, A. Calabrese, C. Carbonera, G. Corso and A. Pellegrino, *Energy Environ. Sci.*, 2014, **7**, 925–943.
53 M. Manceau, S. Chambon, A. Rivaton, J. L. Gardette, S. Guillerez and N. Lematre, *Sol. Energy Mater. Sol. Cells*, 2010, **94**, 1572–1577.
54 H. Huang, Q. Li, M. Qiu, Z. Wang, X. Zhang, S. Liu, N. Fu, B. Zhao, R. Yang and W. Huang, *RSC Adv.*, 2016, **6**, 45873–45883.
55 H. Huang, M. Qiu, Q. Li, S. Liu, X. Zhang, Z. Wang, N. Fu, B. Zhao, R. Yang and W. Huang, *J. Mater. Chem. C*, 2016, **4**, 5448–5460.
56 S. Liu, X. Shi, Y. Hu, X. Zhang, W. Sun, Y. Qi, N. Fu, B. Zhao and W. Huang, *Tetrahedron Lett.*, 2016, **57**, 4452–4455.
57 B. Zhao, C. Yan, Z. Wang, H. Huang, Y. Hu, P. Cheng, M. Yi, C. Huang, X. Zhan and W. Huang, *J. Mater. Chem. C*, 2017, **5**, 8988–8998.
58 X. Shi, S. Liu, C. Liu, Y. Hu, S. Shi, N. Fu, B. Zhao, Z. Wang and W. Huang, *Chem. – Asian J.*, 2016, **11**, 2188–2200.
59 X. Zhou, J. Lu, H. Huang, Y. Yun, Z. Li, F. You, B. Zhao, T. Qin, D. Gao and W. Huang, *Dyes Pigm.*, 2019, **160**, 16–24.
60 F. You, X. Zhou, H. Huang, Y. Liu, S. Liu, J. Shao, B. Zhao, T. Qin and W. Huang, *New J. Chem.*, 2019, **42**, 15079–15087.
61 K. Wong, T. Chao, L. Chi and Y. Chu, *Org. Lett.*, 2006, **8**, 5033–5036.
62 H. Huang, G. Jiao, S. Liu, Q. Li, X. Shi, N. Fu, L. Wang, B. Zhao and W. Huang, *Chem. Commun.*, 2015, **51**, 15846–15849.
63 X. Guo, C. Cui, M. Zhang, L. Huo, Y. Huang, J. Hou and Y. Li, *Energy Environ. Sci.*, 2012, **5**, 7943–7949.

